Journal of Modern Physics, 2024, 15, 480-490
https://www.scirp.org/journal/jmp
ISSN Online: 2153-120X
ISSN Print: 2153-1196

Tunable Multichannel Quantum Routing of Single Photons Based on Single-Mode Microresonators

Jinsong Huang*, Jinglan Hu, Hongwu Huang

School of Information Engineering, Jiangxi University of Science and Technology, Ganzhou, China
Email: *jshuangjs@126.com

How to cite this paper: Huang, J.S., Hu, J.L. and Huang, H.W. (2024) Tunable Multichannel Quantum Routing of Single Photons Based on Single-Mode Microresonators. *Journal of Modern Physics*, **15**, 480-490.
https://doi.org/10.4236/jmp.2024.154023

Received: February 21, 2024
Accepted: March 25, 2024
Published: March 28, 2024

Abstract

We have suggested a novel multiport quantum router of single photons with reflection feedback, which is formed by three waveguides coupled with four single-mode microresonators. The single-photon routing probabilities of four channels in the coupled system are studied theoretically by applying the real-space approach. Numerical results indicate that unidirectional routing in these output channels can be effectively implemented, and the router is tunable to route desired frequencies into the output ports, by varying the inter-resonator detunings via spinning resonator technology. Therefore, the proposed multichannel system can provide potential applications in optical quantum communication.

Keywords

Quantum Routing, Scattering Theory, Optical Waveguide, Microresonators

1. Introduction

In recent years, quantum network, as a kind of important building block for quantum information processing, has become one part of the increasingly exciting fields in quantum physics and information science, since it is applied to effectively transfer quantum signals and link quantum computers via communication channels [1]. Typically, quantum networks are composed of quantum channels and quantum nodes, where the quantum channels are provided by one-dimensional optical waveguides, while single photons are transmitted on the guided channels as quantum information carriers. As a key element of quantum node, quantum router distributes quantum signals to different quantum channels by controlling the interactions between guided waves and emitters. Conse-

quently, various studies have been carried out on quantum routing of single photons in the waveguide quantum electrodynamics systems with coupled components, including atomic qubits [2] [3] [4] [5] [6], quantum dots [7] [8] [9] [10] [11], optomechanical systems [12] [13], whispering gallery resonators (WGRs) [14] [15], cavity (circuit) quantum electrodynamics [16] [17] [18] [19], and chiral systems [20] [21] [22] [23], etc.

Since a quantum network is usually a multichannel system, quantum routers are required to manipulate the transmission of photons from one channel to the others. For the multichannel system, it is thus of considerable importance to provide a controllable path to allow users to route the desired frequencies to the output channel at high transfer rates. Recently, several schemes of multichannel quantum routing have been proposed, by linking more quantum emitters to the output ports in the branch waveguides. In these proposes, low single-photon routing rates from the input waveguide to other numerous output ports are presented [8] [9] [10], which may restrict their more potential applications. To improve the routing probability, the reflectors or phase shifters with high-precision locations are attached to the bus waveguides [5] [6] [11], which leads to the complexity of these structures.

Inspired by these considerations, we propose a novel four-channel router composed of a three-waveguide system with a reflector, in which the bus waveguide and other two drop waveguides are connected mediately by four single-mode WGRs. The incident photons are transferred to two ports in the drop waveguides, meanwhile, the reflector is used to reflect the forward photons and redirect them to other two ports. With such a structure, the crosstalk effects between different frequencies are suppressed, and multiple peak frequencies in the four-channel structure with high routing efficiency of approximately 1 can be achieved on demand, by adjusting the inter-resonator detunings via spinning resonator technology. Moreover, the reflector and resonators are independent of their exact positions, which is helpful to reduce the complexity of the router. Therefore, the proposed multichannel system may be exploited in optical quantum communication.

2. Theoretical Model

Schematic view of a four channel router is sketched in **Figure 1**. It consists of a bus waveguide-a and two drop waveguides-(b,c), and they are connected by four coupled single-mode whispering-gallery resonators to generate four waveguide-waveguide channels. These resonators are described by the creation operator $e_n^{\dagger}$ ($n=1,2,3,4$ through the paper), with the transition frequency ω_n. The coupling strength for four resonators and the bus waveguide is denoted as V_{an}. Similarly, V_{bn} describes the coupling strength for these resonators and these drop waveguides. In the routing structure, a perfect reflecting mirror at the position $x=d_2$ is also used to add the routing channel. The input photons from the left port of the bus waveguide are directly coupled to the resonators R_1

and R_2 located at $x=0$, and then dropped to two left ports in the drop waveguides, whereas these photons moving forward are reflected back by the mirror, and then redirected to two right ports of the drop waveguide by coupling two resonators R_3 and R_4 located at $x=d_1$, via the mode-direction matching of the guided-wave and resonator modes [24].

The total Hamiltonian in the real space [24] of the system can be written by ($\hbar=1$)

$$\begin{aligned} H = & \sum_{m=a,b,c}\int \mathrm{d}x\left[-i\upsilon_g C_{Rm}^{\dagger}(x)\frac{\partial}{\partial x}C_{Rm}(x)+i\upsilon_g C_{Lm}^{\dagger}(x)\frac{\partial}{\partial x}C_{Lm}(x)\right] \\ & +\sum_{n=1,2,3,4}(\omega_n-i\gamma_n)e_n^{\dagger}e_n+\sum_{p=1,2}V_{ap}\int \mathrm{d}x\,\delta(x)\left[C_{Ra}^{\dagger}(x)e_p+C_{Ra}(x)e_p^{\dagger}\right] \\ & +\sum_{s=3,4}V_{as}\int \mathrm{d}x\,\delta(x-d_1)\left[C_{Ra}^{\dagger}(x)e_s+C_{Ra}(x)e_s^{\dagger}\right] \\ & +\int \mathrm{d}x\,\delta(x)\left\{V_{b1}\left[C_{Lb}^{\dagger}(x)e_1+C_{Lb}(x)e_1^{\dagger}\right]+V_{c2}\left[C_{Lc}^{\dagger}(x)e_2+C_{Lc}(x)e_2^{\dagger}\right]\right\} \\ & +\int \mathrm{d}x\,\delta(x-d_1)\left\{V_{b3}\left[C_{Rb}^{\dagger}(x)e_3+C_{Rb}(x)e_3^{\dagger}\right]+V_{c4}\left[C_{Rc}^{\dagger}(x)e_4+C_{Rc}(x)e_4^{\dagger}\right]\right\}. \end{aligned} \tag{1}$$

Here, $C_{Rm}^{\dagger}(x)\left[C_{Lm}^{\dagger}(x)\right]$ denotes the bosonic operator generating a right-moving (left-moving) photon at x in the waveguide-m. υ_g is the group velocity of the propagating photon with the input frequency ω. $\delta(x)\left[\delta(x-d_1)\right]$ means that the resonator-waveguide interaction occurs at $x=0(d_1)$. γ_n stands for the energy dissipation of these resonators.

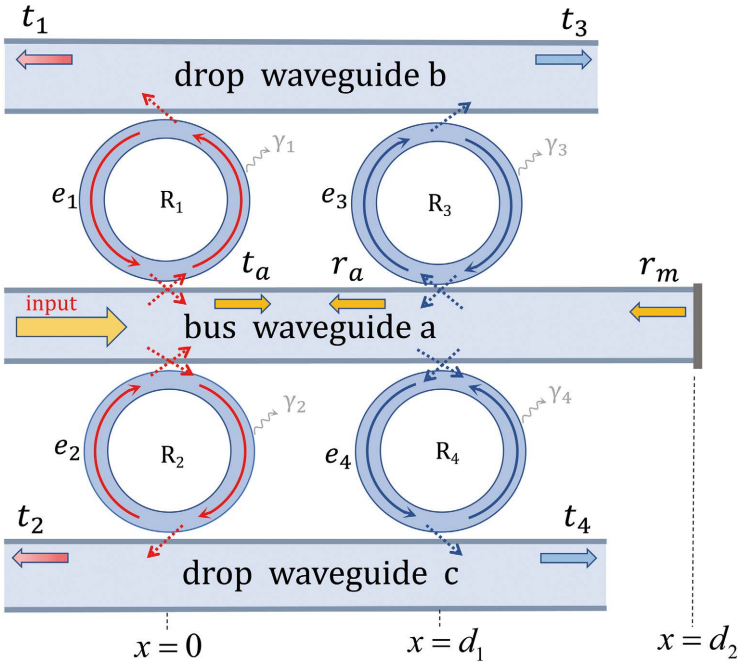

Figure 1. (Color online) Schematic configuration of a single-photon quantum router made of a bus waveguide, two drop waveguides, and four coupled single-mode WGRs (R_n). One end of the bus waveguide is terminated by a perfect reflecting mirror located at $x=d_2$, to reflow the forward photons to couple the two resonators R_3 and R_4. The ingoing photon from the left in the bus waveguide will be coupled with four microresonators, and are transferred to four output ports in the drop waveguides.

Assume that a single photon is incident from the left in the bus waveguide with the energy $E_k = \omega$, then the eigenstate of the Hamiltonian (1), defined by $H|\psi\rangle = E_k|\psi\rangle$, can be expressed in the form:

$$|\psi\rangle = \sum_{m=a,b,c} \int \mathrm{d}x \left[\phi_{Rm}(x) C_{Rm}^{\dagger}(x) + \phi_{Lm}(x) C_{Lm}^{\dagger}(x)\right] |\varnothing\rangle + \sum_{n=1,2,3,4} \xi_n e_n^{\dagger} |\varnothing\rangle. \quad (2)$$

Here, $|\varnothing\rangle$ means that these guided modes and resonator modes are all in their vacuum states with zero photons. ϕ_{Rm} and ϕ_{Lm} represent the wave functions of guided modes in the left and right directions of these waveguide channels, respectively, and ξ_n stands for the excitation probability amplitude of photons in the nth resonator. Their according wave functions take the forms:

$$\begin{aligned}
\phi_{Ra} &= \mathrm{e}^{ikx}\theta(-x) + \mathrm{e}^{ikx} t_a \theta(x), \\
\phi_{La} &= \mathrm{e}^{-ikx} r_a \theta(d_1 - x) + \mathrm{e}^{-ikx} r_m \theta(x - d_1), \\
\phi_{Lb} &= \mathrm{e}^{-ikx} t_1 \theta(-x), \\
\phi_{Lc} &= \mathrm{e}^{-ikx} t_2 \theta(-x), \\
\phi_{Rb} &= \mathrm{e}^{ikx} t_3 \theta(x - d_1), \\
\phi_{Rc} &= \mathrm{e}^{ikx} t_4 \theta(x - d_1).
\end{aligned} \quad (3)$$

Here, t_a and r_a represent the transmission and reflection amplitudes in the bus waveguide channel, respectively. r_m is the reflection amplitude from the mirror reflection. t_1 and t_3 describe the transmission amplitudes in the waveguide-b, while t_2 and t_4 describe the transmission amplitudes in the waveguide-c. $\theta(x)$ denotes the Heaviside step function, with $\theta(0) = 1/2$.

Using the boundary condition $\phi_{Ra}(d_2) + \phi_{La}(d_2) = 0$ at the right port of the bus waveguide, we can obtain the scattering amplitudes as follows:

$$\begin{aligned}
t_a &= 1 - 2i \frac{\Gamma_{a1} Q_2 + \Gamma_{a2} Q_1}{(Q_1 + i\Gamma_{a1})(Q_2 + i\Gamma_{a2}) + \Gamma_{a1}\Gamma_{a2}}, \\
r_a &= \mathrm{e}^{2ikd_2} \left[2i \frac{\Gamma_{a3} Q_4 + \Gamma_{a4} Q_3}{(Q_3 + i\Gamma_{a3})(Q_4 + i\Gamma_{a4}) + \Gamma_{a3}\Gamma_{a4}} - t_a \right], \\
t_1 &= \frac{-2i\sqrt{\Gamma_{a1}\Gamma_{b1}} Q_2}{(Q_1 + i\Gamma_{a1})(Q_2 + i\Gamma_{a2}) + \Gamma_{a1}\Gamma_{a2}}, \\
t_2 &= \frac{-2i\sqrt{\Gamma_{a2}\Gamma_{c2}} Q_1}{(Q_1 + i\Gamma_{a1})(Q_2 + i\Gamma_{a2}) + \Gamma_{a1}\Gamma_{a2}}, \\
t_3 &= 2i\mathrm{e}^{2ik(d_2 - d_1)} \frac{\sqrt{\Gamma_{a3}\Gamma_{b3}} Q_4}{(Q_3 + i\Gamma_{a3})(Q_4 + i\Gamma_{a4}) + \Gamma_{a3}\Gamma_{a4}} t_a, \\
t_4 &= 2i\mathrm{e}^{2ik(d_2 - d_1)} \frac{\sqrt{\Gamma_{a4}\Gamma_{c4}} Q_3}{(Q_3 + i\Gamma_{a3})(Q_4 + i\Gamma_{a4}) + \Gamma_{a3}\Gamma_{a4}} t_a.
\end{aligned} \quad (4)$$

Here, $\Gamma_{an} = V_{an}^2 / (2\upsilon_g)$, $\Gamma_{bn} = V_{bn}^2 / (2\upsilon_g)$, and $\Gamma_{cn} = V_{cn}^2 / (2\upsilon_g)$.

$Q_1 = \Delta\omega + i\gamma_1 + i\Gamma_{b1}$, $Q_2 = \Delta\omega + \Delta\omega_{12} + i\gamma_2 + i\Gamma_{c2}$, $Q_3 = \Delta\omega + \Delta\omega_{13} + i\gamma_3 + i\Gamma_{b3}$, and $Q_4 = \Delta\omega + \Delta\omega_{14} + i\gamma_4 + i\Gamma_{c4}$. $\Delta\omega = \omega - \omega_1$ is the frequency detuning between the incident photon frequency and the resonator-1, and $\Delta\omega_{1n} = \omega_1 - \omega_n$ is the frequency detuning between the first and *n*th resonator.

3. Quantum Routing of Single Photons in the Coupled System

To investigate the routing properties in the proposed system, we will examine the scattering probabilities in the coupled system, which are denoted as $T_{a(1,2,3,4)} = \left|t_{a(1,2,3,4)}\right|^2$ and $R_a = \left|r_a\right|^2$. For comparison, we first consider the case in which only the resonator-1 is coupled to the bus waveguide. Here, the resonator-waveguide coupling ratio $P = \Gamma_{b1}/\Gamma_{a1}$ is set. For simplification, all the parameters are in units of the coupling Γ_{a1}. When a single photon is incident from the left side of the bus waveguide, it will pass through the bus waveguide, and is reflected back by the reflector. It also will transmit to the drop waveguide-1 on resonance, as seen in **Figure 2(a)** and **Figure 2(b)** and demonstrated by Monifi *et al.* [25], where single drop peaks of T_1 are exhibited at the resonance point $\Delta\omega = 0$ for different resonator-waveguide couplings. Under the condition of $P_b = 1$ and zero dissipation $\gamma_1 = 0$, the maximum drop peak with routing rate of unity is available, which means that the moving photon along the bus waveguide is completely blocked by the coupled resonator-1, and then wholly dropped to output port of the waveguide-1. This scenario results from the effect of two symmetrical coupled paths created by the equal resonator-waveguide couplings $\Gamma_{b1} = \Gamma_{a1}$, through which the whole transfer between two waveguides can be achieved. It is also found that the photon-flow conservation relation $R_a + T_1 = 1$ (see the yellow straight line) in two ports is kept for any incident frequencies when no dissipations are included.

When another three waveguides are coupled to the bus waveguide through the additional coupled resonators, four output channels are open. The scattering spectra of single photons versus $\Delta\omega$ in four output ports are presented in **Figure 2(c)**, as seen that four drop peaks with unities at the central frequency locations of $\Delta\omega_n$ appear for the appropriate inter-resonator detunings $\Delta\omega_{12} = \Delta\omega_{23} = \Delta\omega_{34} = 25$, which implies our proposed system can be utilized as a unidirectional quantum router. Furthermore, the effect of the resonator-waveguide couplings on four drop peaks is shown in **Figure 2(d)**. For simplification, $P = \Gamma_{bn}/\Gamma_{an}$ is here taken as the coupling ratio, and assumed to be the same. As seen, four drop peaks in these channels emerge in four dark-red regions for these equal resonator-waveguide couplings, where a white straight line with $P = 1$ passes through these bulge points. Similar to the above single-resonator case, more symmetrical transmission paths among these waveguides and resonators are formed, and result in more complete transfers of the input frequencies.

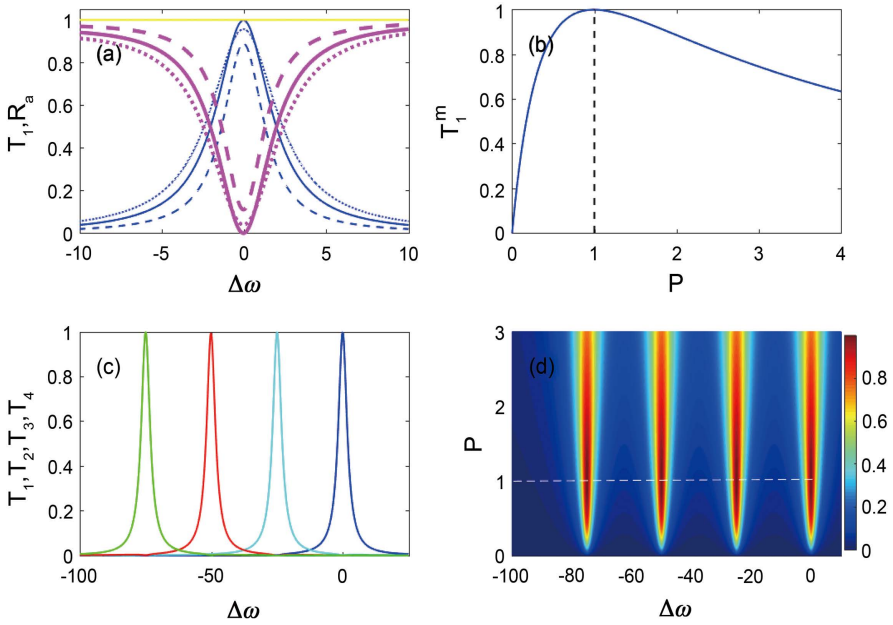

Figure 2. (Color online) (a) The transfer T_1 (thin blue curves) and the reflection R_a (thick pink curves) for different coupling ratios: $P=0.5$ (dashed curves), $P=1$ (solid curves), and $P=1.5$ (dotted curves). (b) The maximum transfer peak T_1^m versus the coupling ratio P. (c) The transfer T_1, T_2, T_3, and T_4 (from the right to left) in the four channels with the equal inter-resonator detunings $\Delta\omega_{12}=\Delta\omega_{23}=\Delta\omega_{34}=25$. (d) T_1, T_2, T_3, and T_4 (from the right to left) as a function of P and $\Delta\omega$. Zero dissipation ($\gamma_1=0$) is taken. For convenience, all the parameters are in units of Γ_{a1}.

Next, we consider the effect of the inter-resonator detunings on the transfer rates in the routing spectra of the incident photons. When more transmission channel emerges, the crosstalk of different signals is generated accordingly due to the photon interference, which will result in low routing efficiencies of the input frequencies. As shown in **Figure 3(a)**, the minimum peak values of T_n emerge at the resonance site $\omega_1=\omega_2=\omega_3=\omega_4$, where the strongest interference occurs. T_1 and T_2 overlap with the minimum routing probability of about 0.44, which is a general peak value at resonances for a multichannel routing system coupled with multiple single-mode excited emitters [6]. T_3 and T_4 also overlap with lesser routing probability of 0.12, due to the fact that transmission photons in the right two channel come from the reflected parts, and suffer more interferences from the reflecting mirror. For simplification, the inter-resonator detunings $\Delta\omega_{23}=\Delta\omega_{34}=\Delta\omega_{12}$ are supposed here. When varying the inter-resonator detuning $\Delta\omega_{12}$, it is obvious that the crosstalk decreases sharply with the increase of $\Delta\omega_{12}$, and the peak values of the scattering spectra reach rapidly the maximum output value of unities, as displayed in **Figure 3(b)** and **Figure 3(c)**. **Figure 3(d)** shows that the drop peak of T_1 at the resonance point ω_1 gets higher when increasing the inter-resonator detuning, while their corresponding loss $C_{2(3,4)}$ induced from the crosstalk of other signals reduce to zeros around $\Delta\omega_{12}=10$.

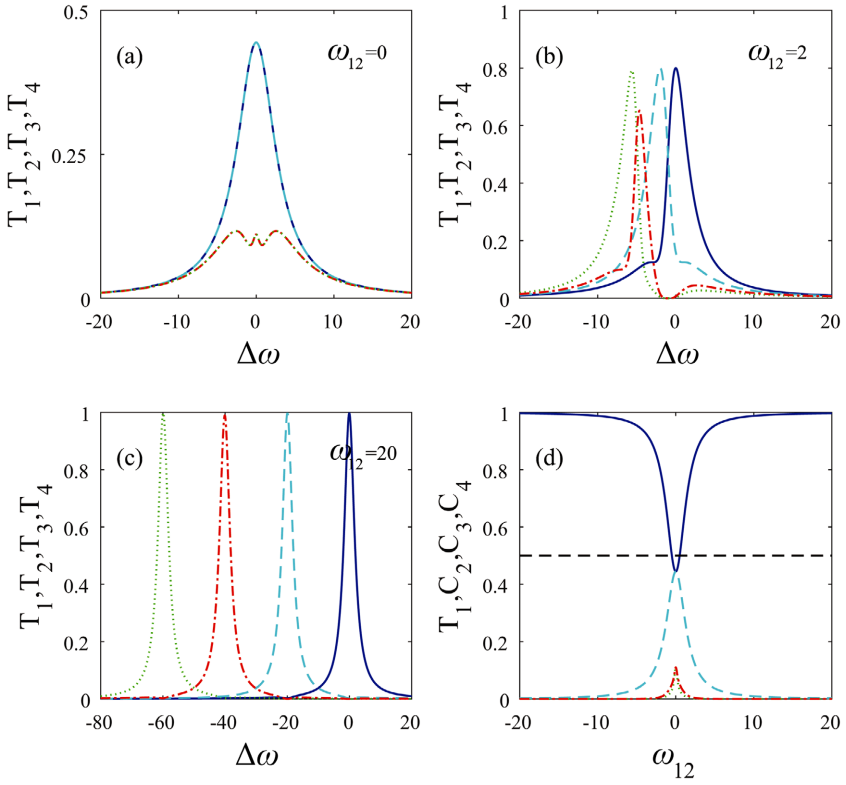

Figure 3. (Color online) The transfer T_1 (solid blue curves), T_2 (dashed cyan curves), T_3 (dash dotted red curves), and T_4 (dotted green curves) for different inter-resonator detunings: $\Delta\omega_{12}=0$ in (a), $\Delta\omega_{12}=2$ in (b), and $\Delta\omega_{12}=20$ in (c). (d) The transfer peak T_1 (solid blue line) and the corresponding losses C_2 (dashed cyan line), C_3 (dash dotted red line), and C_4 (dotted green line) induced by the crosstalk versus the inter-resonator detuning $\Delta\omega_{12}$. Here, $P=1$, $\Delta\omega_{12}=\Delta\omega_{23}=\Delta\omega_{34}$ and $\gamma_1=\gamma_2=\gamma_3=\gamma_4=\gamma_0=0$ are set.

To gain a deeper insight into the effect of the inter-resonator detunings on the routing efficiencies of four drop ports, **Figure 4(a)** plots the drop peak spectra for four channels verus different inter-resonator detunings and their central frequency locations. The peaks T_1^m and T_2^m overlap and go acutely up from the minimum routing probability of 0.44 to the maximum value of one, similarly T_3^m and T_4^m vary from 0.12 to 1 as inter-resonator detuning $\Delta\omega_{12}$ becomes bigger. **Figure 4(b)** also displays that these drop peaks with maximal values of unities are exhibited in four different narrow and straight dark-red windows. The drop peak of T_1 is fixed at ω_1 and presented vertically, while the central frequencies of another three channels expand obliquely with a frequency shift equal to the inter-resonator detuning for each channel signal.

Experimentally, the inter-resonator detunings can be controlled by rotating the resonators [26] [27] [28]. For a rotary resonator with an angular velocity Ω, the light circulating in the spinning resonator suffers a Fizeau shift related to the angular velocity, which can result in a detuing from the resonance frequency of the nonspinning resonator. Consequently, controlling the inter-resonator detuning can serve as a novel route to implement highly-efficient routing of mul-

tiple channels, because the widened frequency intervals can suppress effectively the interference and crosstalk from these transmission signals.

Note that these channel routings are independent of the determined locations of these resonators and the reflector, as indicated in Equation (3) that the exponential terms related to the locations are eliminated under the action of modular square to obtain the routing probabilities, since the mode-direction matching condition is satisfied by the horizontal propagating and reflection direction of the photons and rotary mode direction of the resonator. Compared with the previous schemes requiring the precise phase shifts related to the reflector locations [5] [6] [11] to obtain more high transfer probabilities, the proposed routers needing no accurate positions have some advantages.

In the above discussions, the dissipations are not considered. In a practical experiment, the routing system inevitably suffers losses from the resonators. **Figure 5(a)** describes the effect of the dissipations on the routing efficiencies for the coupled waveguide. Obviously, all transfer rates of four channels decrease as the dissipations are increased, in comparison with the routing spectra without dissipations. Complete photon transfer can not emerge even for the symmetrical coupled routes owing to the photon leakage, which results in the shifts of the coupling ratio P to determine the maximum transfer peaks. As seen in **Figure 5(b)**, increasing the resonator intrinsic losses decreases the maximum peak values and shifts P to higher values, for instance, strong dissipation such as $\gamma = \Gamma_a$ leads to a remarkable shift of around $P = 1.5$. Here, equal dissipations $\gamma_n = \gamma_0$ are taken. However, for high-quality resonators with very-low losses, high transfer rates of T_n are still available, such as the expected results about 0.95 for $\gamma_0 = 0.05$.

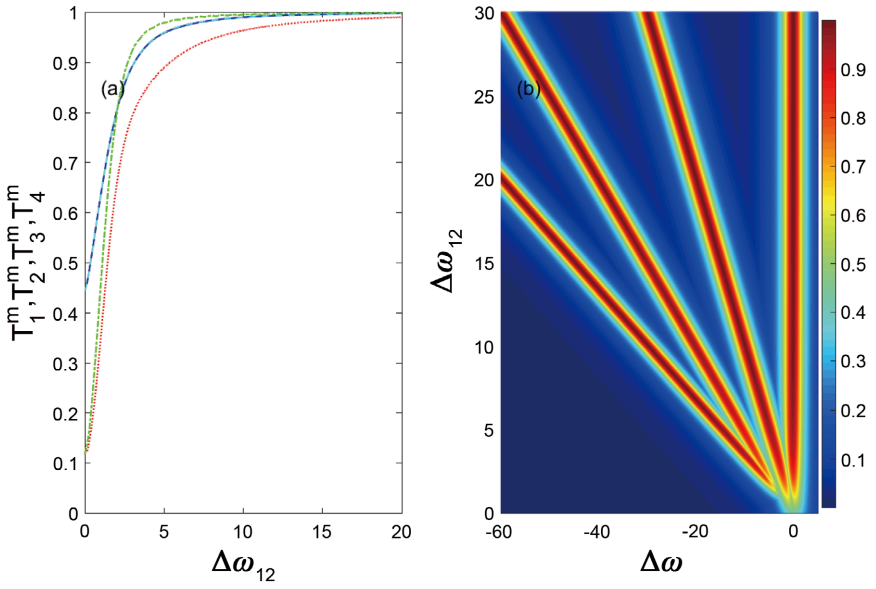

Figure 4. (Color online) (a) The maximum transfer peaks T_1^m (thin blue curve), T_2^m (dashed cyan curve), T_3^m (dash dotted red curve), and T_4^m (dotted green curve) versus the inter-resonator detuning $\Delta\omega_{12}$. (b) T_1, T_2, T_3, and T_4 (from the right to left) as a function of $\Delta\omega_{12}$ and $\Delta\omega$. These parameters are $P = 1$ and $\gamma_0 = 0$.

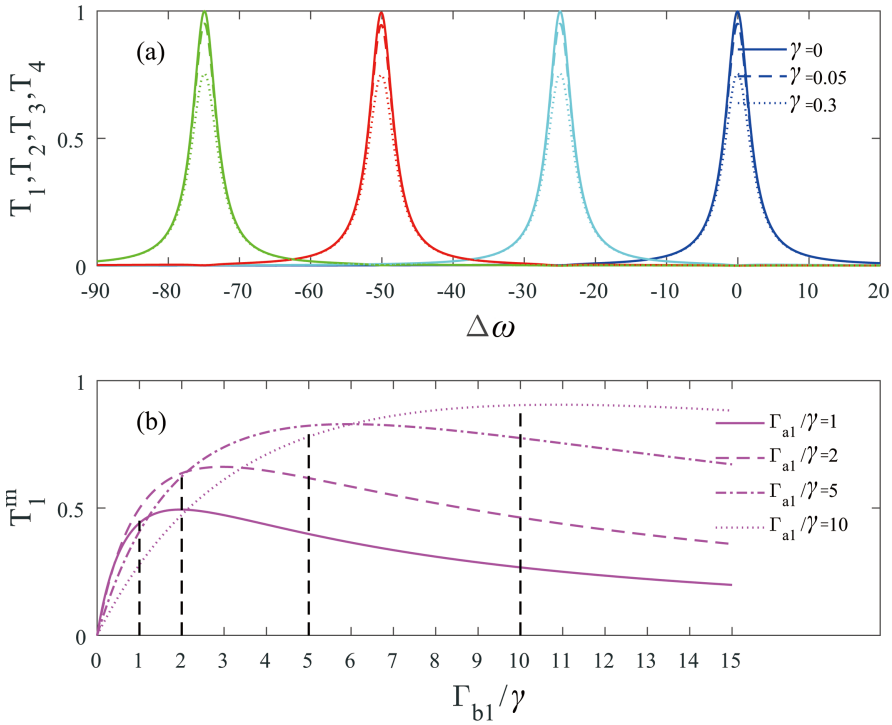

Figure 5. (Color online) (a) T_1, T_2, T_3, and T_4 (from the right to left) for different dissipations: $\gamma_0 = 0$ (solid lines), $\gamma_0 = 0.05$ (dashed lines), and $\gamma_0 = 0.3$ (dotted lines). (b) The dependence of the maximum routing efficiency T_1^m on the resonator intrinsic loss and waveguide-resonator couplings. These parameters are $P = 1$ and $\Delta\omega_{12} = 25$.

4. Conclusion

In summary, we have investigated the quantum routing of single photons in a coupled four-channel waveguide system with a reflecting mirror. Using a real-space approach, the photon scattering amplitudes in these ports are derived exactly. Our results show that high routing capabilities over these channels are available, and the router is tunable to route photons into any output channels on demand, by adjusting the parameters. Our multichannel scheme for routing single photons could be utilized to realize other quantum devices, such as filters, switches, and demultiplexers, etc.

Acknowledgements

This work was supported by Jiangxi Provincial Natural Science Foundation (Grant No. 20212BAB201014).

Conflicts of Interest

The authors declare no conflicts of interest regarding the publication of this paper.

References

[1] Kimble, H.J. (2008) *Nature* (*London*), **453**, 1023-1030.

https://doi.org/10.1038/nature07127

[2] Shomroni, I., Rosenblum, S., Lovsky, Y., Brechler, O., Guendelman, G. and Dayan, B. (2014) *Science*, **345**, 903-906. https://doi.org/10.1126/science.1254699

[3] Li, X.M. and Wei, L.F. (2015) *Physical Review A*, **92**, Article ID: 063836. https://doi.org/10.1103/PhysRevA.92.063836

[4] Huang, J.S., Wang, J.W., Wang, Y., Li, Y.L. and Huang, Y.W. (2018) *Quantum Information Processing*, **17**, Article No. 78. https://doi.org/10.1007/s11128-018-1850-9

[5] Huang, J.S., Zhong, J.T., Li, Y.L., Xu, Z.H. and Xiao, Q.S. (2020) *Quantum Information Processing*, **19**, Article No. 290. https://doi.org/10.1007/s11128-020-02789-0

[6] Wu, J.N., Dong, J., Xu, Y., Zou, B. and Zhang, Y. (2022) *Physical Review Applied*, **18**, Article ID: 054007. https://doi.org/10.1103/PhysRevApplied.18.054007

[7] Hu, C.Y. (2016) *Physical Review B*, **94**, Article ID: 245307. https://doi.org/10.1103/PhysRevB.94.245307

[8] Ko, M.C., Kim, N.C. and Choe, H. (2019) *Physica Scripta*, **94**, Article ID: 125605. https://doi.org/10.1088/1402-4896/ab241a

[9] Ko, M.C., Kim, N.C., Choe, H., Ri, S.R., Ryom, J.S., Ri, C.W. and Kim, U.H. (2020) *Plasmonics*, **15**, 271-277. https://doi.org/10.1007/s11468-019-01022-8

[10] Kim, N.C., Ko, M.C., Ryom, J.S., Choe, H., Choe, I.H., Ri, S.R. and Kim, S.G. (2021) *Quantum Information Processing*, **20**, Article No. 5. https://doi.org/10.1007/s11128-020-02884-2

[11] Kim, N.C., Kim, C.M., Ko, M.C., Ryom, J.S., Ri, G.Y., Ryom, G.M. and Kim, Y.J. (2023) *Quantum Information Processing*, **22**, Article No. 21. https://doi.org/10.1007/s11128-022-03722-3

[12] Agarwal, G.S. and Huang, S. (2012) *Physical Review A*, **85**, Article ID: 021801. https://doi.org/10.1103/PhysRevA.85.021801

[13] Li, X., Zhang, W.Z., Xiong, B. and Zhou, L. (2016) *Scientific Reports*, **6**, Article No. 39343. https://doi.org/10.1038/srep39343

[14] Aoki, T., Parkins, A.S., Alton, D.J., Regal, C.A., Dayan, B., Ostby, E., Vahala, K.J. and Kimble, H.J. (2009) *Physical Review Letters*, **102**, Article ID: 083601. https://doi.org/10.1103/PhysRevLett.102.083601

[15] Cao, C., Duan, Y.W., Chen, X., Zhang, R., Wang, T.J. and Wang, C. (2017) *Optics Express*, **25**, 16931-16946. https://doi.org/10.1364/OE.25.016931

[16] Hoi, I.C., Wilson, C.M., Johansson, G., Palomaki, T., Peropadre, B. and Delsing, P. (2011) *Physical Review Letters*, **107**, Article ID: 073601.

[17] Xia, K. and Twamley, J. (2013) *Physical Review X*, **3**, Article ID: 031013. https://doi.org/10.1103/PhysRevX.3.031013

[18] Zhou, L., Yang, L.P., Li, Y. and Sun, C.P.(2013) *Physical Review Letters*, **111**, Article ID: 103604. https://doi.org/10.1103/PhysRevLett.111.103604

[19] Huang, J.S., Wang, J.W., Li, Y.L., Wang, Y. and Huang, Y.W. (2019) *Quantum Information Processing*, **18**, Article No. 59. https://doi.org/10.1007/s11128-019-2176-y

[20] Gonzalez-Ballestero, C., Moreno, E., Garcia-Vidal, F.J. and Tudela, A.G. (2016) *Physical Review A*, **94**, Article ID: 063817. https://doi.org/10.1103/PhysRevA.94.063817

[21] Cheng, M.T., Ma, X.R., Fan, J.W., Xu, J.P. and Zhu, C.J. (2017) *Optics Letters*, **45**, 2914-2917. https://doi.org/10.1364/OL.42.002914

[22] Yan, C.H., Li, Y., Yuan, H.D. and Wei, L.F. (2018) *Physical Review A*, **97**, Article ID: 023821. https://doi.org/10.1103/PhysRevA.97.023821

[23] Yan, W.B., Ni, W.Y., Zhang, J., Zhang, F.Y. and Fan, H. (2018) *Physical Review A*, **98**, Article ID: 043852. https://doi.org/10.1103/PhysRevA.98.043852

[24] Shen, J.T. and Fan, S. (2009) *Physical Review A*, **79**, Article ID: 023838. https://doi.org/10.1103/PhysRevA.79.023838

[25] Monifi, F., Özdemir, Ş.K. and Yang, L. (2013) *Applied Physical Letters*, **103**, Article ID: 181103. https://doi.org/10.1063/1.4827637

[26] Maayani, S., Dahan, R., Kligerman, Y., Moses, E., Hassan, A.U., Jing, H., Nori, F., Christodoulides, D.N. and Carmon, T. (2018) *Nature* (*London*), **558**, 569-572. https://doi.org/10.1038/s41586-018-0245-5

[27] Huang, R., Miranowicz, A., Liao, J.Q., Nori, F. and Jing, H. (2018) *Physical Review Letters*, **121**, Article ID: 153601. https://doi.org/10.1103/PhysRevLett.121.153601

[28] Li, B., Huang, R., Xu, X., Miranowicz, A. and Jing, H. (2019) *Photonics Research*, **7**, 630-641. https://doi.org/10.1364/PRJ.7.000630